THE ASTROPHYSICAL JOURNAL, 578:L149–L152, 2002 October 20

STRUCTURE IN THE ϵ ERIDANI DUSTY DISK CAUSED BY MEAN MOTION RESONANCES WITH A 0.3 ECCENTRICITY PLANET AT PERIASTRON

A. C. QUILLEN AND STEPHEN THORNDIKE
Department of Physics and Astronomy, University of Rochester, Rochester, NY 14627-0171; aquillen@pas.rochester.edu, slt3@alfred.edu
Received 2002 August 14; accepted 2002 September 13; published 2002 September 20

ABSTRACT

The morphology of the ϵ Eridani dust ring is reproduced by a numerical simulation of dust particles captured into the 5 : 3 and 3 : 2 exterior mean motion resonances with a 0.3 eccentricity 10^{-4} $M_\odot$ planet at periastron at a semimajor axis of 40 AU. The morphology will differ when the planet is at apastron, in about 140 yr. Moderate eccentricity planets in outer extrasolar systems will cause observable variations in the morphology of associated dusty rings.

Subject headings: circumstellar matter — planetary systems — stars: individual (ϵ Eridani)

On-line material: color figure

1. INTRODUCTION

The *Infrared Astronomical Satellite* measured far-infrared fluxes from the vicinity of main-sequence stars (Aumann et al. 1984), including the nearby systems Vega and Formalhaut, which are of moderate age, 10^8 yr, at the end of the era when rocky planets are expected to form. Recently, submillimeter wavelength images of stars with infrared excesses have revealed structure in some of these disks. Formalhaut has a dust ring with a central cavity (Holland et al. 1998), Vega, β Pictorus, and HR 4796A have secondary dust emission peaks and central cavities (Wilner et al. 2002; Holland et al. 1998; Jayawardhana et al. 1998; Koerner et al. 1998), HR 4796A has a ring evident in scattered light from the central star (Schneider et al. 1999), and ϵ Eridani has a 60 AU dusty ring with four peculiar peaks of emission (Greaves et al. 1998). HR 4796A and β Pic are younger, at ages of only $\sim 10^7$ yr, whereas ϵ Eri (HR 1084) is a nearby 0.5–1 Gyr old K2 V (0.8 $M_\odot$) star (Soderblom & Dappen 1989; Song et al. 2000).

Because of the short lifetime of the dust particles in these disks, and the scarcity of gas, the dust must continually be replenished from collisions of larger orbiting bodies, possibly analogous to Kuiper belt objects. Hence, the disks in the older systems are commonly called debris disks. Dust particles in our solar system spiral toward the Sun owing to radiation drag forces, known as Poynting-Robertson (P-R) drag, and interactions with the solar wind (Burns, Lamy, & Soter 1979). Gravitational perturbations from planets can scatter the particles or capture them into orbital resonances with planets (e.g., Dermott et al. 1994). Since the lifetime of captured particles can greatly exceed the lifetime of particles that are not captured, resonant trapping can sculpt the dusty disk.

Structure predicted in the dust distribution in the Kuiper belt is primarily a result of resonance trapping (Liou & Zook 1999; Moro-Martin & Malhotra 2002). Wilner et al. (2002) suggested that the two peaks seen at 1.3 mm in the Vega disk could be explained by the capture of dust particles into the 2 : 1 exterior mean motion resonance with a high-eccentricity 3 M_J giant planet at a semimajor axis of 40 AU. Ozernoy et al. (2000) proposed that the morphology of the submillimeter images of the ϵ Eri system could be caused by dust particles trapped in high-libration orbits associated with the 3 : 2 mean motion resonances with a $\sim$0.2 M_J planet in a circular orbit. While Ozernoy et al. (2000) considered the morphology caused by dust particles carefully placed in individual resonances, here we initially distribute dust particles over a range of semimajor axes and eccentricities and search for stable dust configurations that can account for the four peaks observed in the submillimeter images of the ϵ Eri system.

2. NUMERICAL INTEGRATION

We numerically integrate the orbits of dust particles using a conventional Burlisch-Stoer numerical scheme. The forces on the particles are gravity from a central star and one planet and P-R drag from the central star. The motion of the dust particles was restricted to the plane containing the planet and star. The ratio of the force from radiation to that from the gravity of the central star is parametrized with the dimensionless parameter, β, which depends primarily on particle size (Burns et al. 1979). Length scales are given in units of the perturbing planet semimajor axis, a_p, and timescales in units such that $GM_* = 1$, where M_* is the mass of the central star. The ratio of the planet mass to the stellar mass is denoted as μ.

Dust particles see a reduced radial force from the central star because radiation pressure opposes gravity. This causes the location of the mean motion resonances with the planet to shift radially by a factor of $(1 - \beta)^{1/3}$. However, the magnitude of the P-R drag force caused by relativistic effects depends on the ratio of the particle velocity to the speed of light, c, times β. Because of our choice of units, the speed of light, c, is in units of $(GM_*/a_p)^{1/2}$. We have adopted $c/(GM_*/a_p)^{1/2} = 5 \times 10^4$, which corresponds to having a stellar mass of 1 $M_\odot$ and a planet radius of 25 AU. Because of the weak dependence of c on stellar mass and planetary semimajor axis, our simulations should scale to outer solar systems, such as the ϵ Eri disk, with the caveat that the particle drift rates should be a factor of a few times lower.

With the exception of Wilner et al. (2002), most simulations of dust dynamics in planetary systems have been carried out for low-eccentricity systems. As Wilner et al. (2002) found, high-eccentricity planets can cause strong azimuthal density contrasts in the distributions of objects trapped in outer resonances, such as the 2 : 1 and 3 : 1 mean motion resonances. Typically we find that the azimuthal contrasts are lower in the outer resonances than those closer to the planet. Previous simulations have predicted that resonances close to the planet such as the 4 : 3, 3 : 2, 5 : 3, and 7 : 4 resonances efficiently trap

and hold dust particles in the Kuiper belt (Liou & Zook 1999; Moro-Martin & Malhotra 2002). We restrict our simulations to the region containing these resonances.

We began the simulations with 300 dust particles distributed randomly in the semimajor axis between 1.1 and 1.5 times the planet's semimajor axis. Longitudes of periastron and mean longitudes were chosen randomly. Dust particle eccentricities were chosen to lie between zero and 0.4. We ran each simulation for 2×10^4 planetary orbit periods. The positions of all the particles were recorded every planetary year; consequently, the phase of the planet was the same during each output of the integration. We binned the particle positions, counting the positions of the particles at each output of the simulation. The resulting spatial distributions and semimajor axis distributions are shown in Figure 1 for the planet at periastron and at apastron. All dust particles contributed to the time-integrated dust distributions; however, particles that were quickly ejected from the system, or quickly impacted the star or planet, contributed less to the integrated dust distributions. Particles that remained trapped in resonances for long periods of time contributed substantially to the dust distribution.

In Figure 1*d*, we show the particle distribution restricted to the semimajor axis between 1.2 and 1.3, containing the 3 : 2 resonance, and between 1.3 and 1.37, containing the 5 : 3 resonance, for the simulations shown in Figures 1*a* and 1*b* when the planet is at periastron and at apastron. Only one family of resonant orbits dominates for both resonances, and the phase of the density peaks with respect to the planet depends on the planet's orbital phase. The distribution of particles in the 3 : 2 resonance exhibits a threefold symmetry, and that of the 5 : 3 exhibits a fivefold symmetry. When the planet is at periastron, the sum of the particle distributions in the 3 : 2 and 5 : 3 resonances exhibits four peaks similar to those observed in the ϵ Eri system.

To simulate the effect of the decreasing radiation field, the dust distribution was weighted by r^{-2}, where r is its radial distance from the star. The resulting predicted intensity image for a planet at periastron, and smoothed to the approximate resolution of the submillimeter observations, is shown in Figure 2 with the submillimeter image by Greaves et al. (1998) for comparison. The dusty disk is tilted assuming a disk inclination of 40° (where 0° corresponds to face-on). This is somewhat higher than the 25° estimated by Greaves et al. (1998) from the ring but consistent with the 30° ± 15° estimated from optical line data (Saar & Osten 1997).

The morphology of the dust simulation shown in Figure 2 exhibits two dominant peaks at mean longitudes of approximately $\pm 3\pi/5$ from the planet, which correspond fairly well to the two dominant peaks southeast and southwest of the star observed in the submillimeter map. Near the planet, a weaker arc is displayed in the simulation, which corresponds to the weaker arc of emission observed to the north of the star in the submillimeter map. However, the dust emission predicted opposite to the planet is more distant from the star than that observed south of the star in the submillimeter image.

In Figure 1*d*, we show particle distributions for restricted ranges of semimajor axes. When the planet is at periastron, density enhancements caused by the 3 : 2 resonance add to those from the 5 : 3 resonance, causing the two dominant peaks seen in Figure 1*a*. When the planet is at apastron, the concentrations caused by the 3 : 2 resonance are out of phase with those in the 5 : 3 resonance. Some substructure is also caused by the 7 : 4 resonance in Figures 1*a* and 1*b*.

In Figures 1 and 2, we have given axes in units of the planet's semimajor axis. The radius of the ring was estimated to be approximately 60 AU, which would correspond to a planet semimajor axis of about two-thirds this, or 40 AU. Assuming a stellar mass of 0.8 $M_\odot$, the planet orbital period is 280 yr. The total time of our simulations (2×10^4 times the planet period) corresponds to 6×10^7 yr.

Dust particles can be trapped in a $k + q : k$ exterior principle mean motion resonance with resonant arguments of the form

$$\phi = (k + q)\lambda - k\lambda_p - p\varpi + (p - q)\varpi_p, \quad (1)$$

where p is an integer between 0 and q, λ and λ_p are the mean longitudes of the particle and planet, respectively, and ϖ and ϖ_p are the longitudes of periastron. We consider the particle to be trapped in the resonance when ϕ librates about a particular fixed value. Take the planet's longitude of periastron as a reference angle ($\varpi_p = 0$). In resonance, the resonance angle $\phi \approx n\pi$, where n is odd if q is even and n is even otherwise.

For the mean longitude of a dust particle very close to the planet to be strongly locked to that of the planet, the resonance responsible is likely to be the $p = 0$ one. In this case,

$$\lambda = \frac{n\pi + k\lambda_p}{k + q}. \quad (2)$$

For the 3 : 2 resonance and when the planet is at periastron ($\lambda_p = \omega_p = 0$), we find dust particles near $\lambda = 0, \pm 2\pi/3$. When the planet is at apastron ($\lambda_p = \pi$), λ is the same. This only looks out of phase in Figure 1*d* because we have rotated the images so that the longitude of the planet is fixed. When the resonant argument ϕ is fixed, we will only find particles with these longitudes, causing the concentrations we see in Figure 1. For the 5 : 3 resonance, when the planet is at periastron, $\lambda = \pi, \pm 3\pi/5, \pm \pi/5$, and when the planet is at apastron, $\lambda = 0, \pm 2\pi/5, \pm 4\pi/5$. This fivefold symmetry is also consistent with the concentrations seen in Figure 1*d*.

In our simulations, we also found particles populating resonances with other values of p; however, these tended to have shorter lifetimes and so contributed less to the final particle distributions. When $p \neq 0$, higher particle densities arise at angles when the particles reach apastron or periastron (see discussion in Wilner et al. 2002). For example, $p = 1$ is favored for the 3 : 2 resonance when the planet is at low eccentricity, causing two peaks in the particle distribution rather than three, which is what is seen in the simulations of Liou & Zook (1999).

3. SUMMARY AND DISCUSSION

We have found that the morphology of dusty material trapped in exterior resonances with a planet can be strongly dependent on the eccentricity and orbital phase of the planet. The morphology of the ϵ Eri dust ring seems to be reproduced by dust particles captured into the 5 : 3 and 3 : 2 exterior resonances with a moderate eccentricity, $e_p \sim 0.3$, planet near periastron. When the planet was more massive ($\mu > 5 \times 10^{-4}$) or more highly eccentric (greater than 0.4), the resonances closest to the planet did not capture and hold particles as efficiently. When the planet mass was below a Saturn mass, the 4 : 3 resonance also contributed to the particle distribution, resulting in four dominant symmetric peaks. The asymmetries observed in the ϵ Eri image were not observed in the dust distribution, so we consider planets less massive than Saturn unlikely to explain the particle distribution. When the planet eccentricity was below 0.15, the azimuthal density variations in the dust distri-

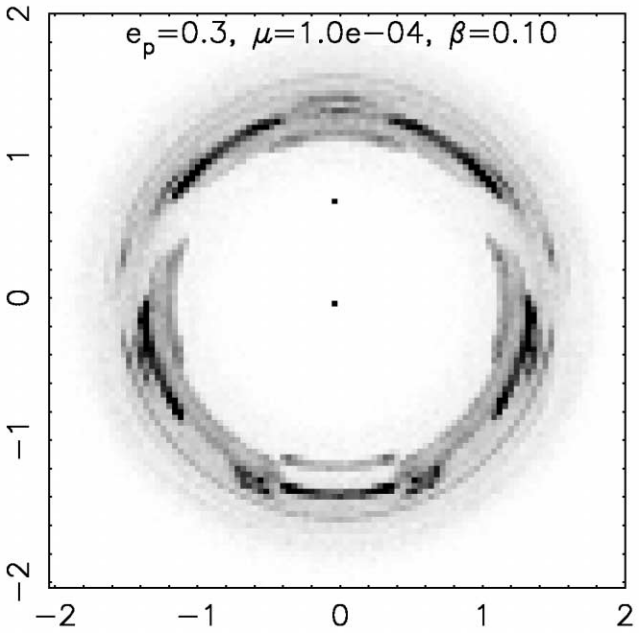

FIG. 1*a*

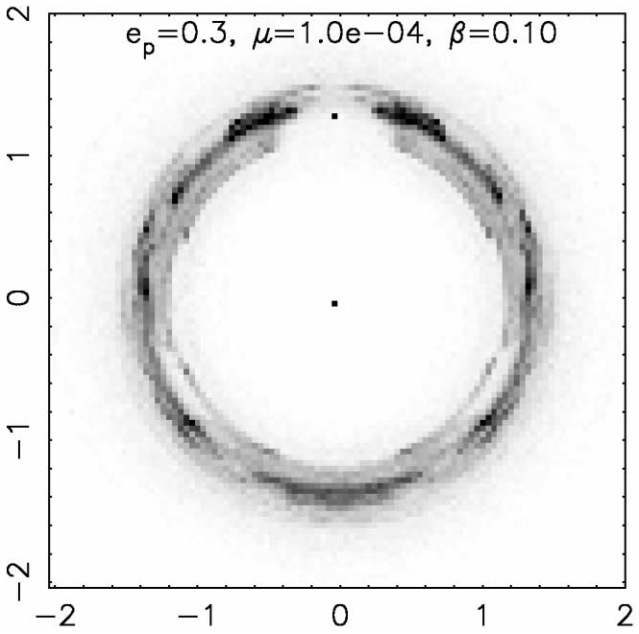

FIG. 1*b*

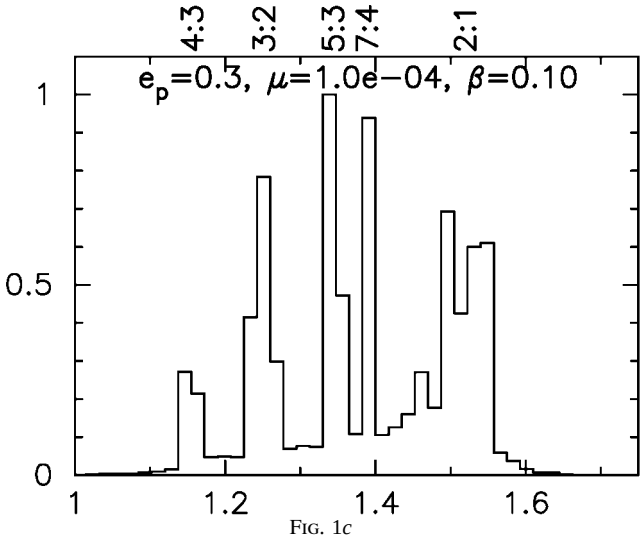

FIG. 1*c*

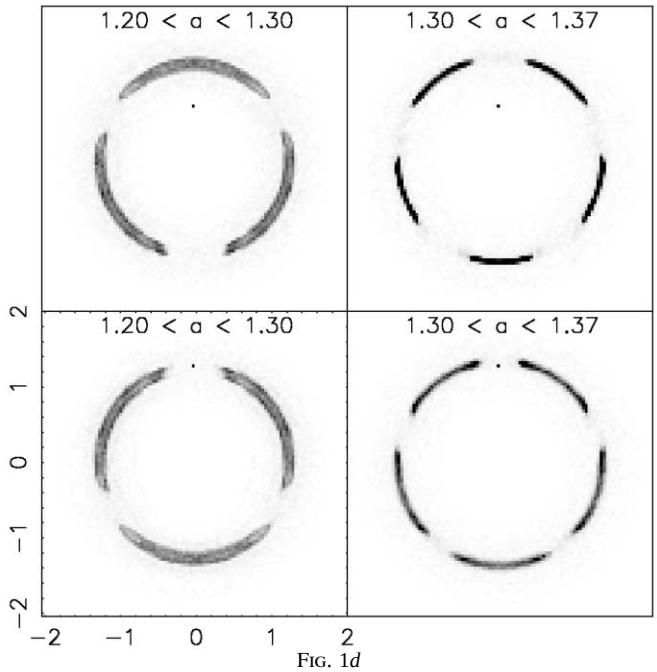

FIG. 1*d*

FIG. 1.—(*a*) Dust distribution for a planet at periastron with a ratio of planet mass to stellar mass $\mu = 10^{-4}$ and eccentricity of $e_p = 0.3$. The dust particles have $\beta = 0.1$. The star and planet are denoted as filled squares at the origin and at a radius of 0.7 from the origin, respectively. Axes are given in units of the planet semimajor axis. (*b*) Same as (*a*), but the planet is at apastron. (*c*) Semimajor axis distribution for the particle distribution shown in (*a*). (*d*) Particle distributions are shown for limited ranges of semimajor axes for the simulations displayed in Figs. 1*a* and 1*b*. Particles in the 3 : 2 resonance are shown for the planet at periastron (*top left*) and at apastron (*bottom left*). Particles in the 5 : 3 resonance are shown for the planet at periastron (*top right*) and at apastron (*bottom right*).

bution were too low to account for the morphology in the ϵ Eri disk.

Our model differs from that proposed by Ozernoy et al. (2000) in a number of ways. The period of the orbital planet in our model is 280 yr, which should cause the pattern to revolve about the star by $\sim 1\overset{\circ}{.}3\ \mathrm{yr}^{-1}$, faster than the $\sim 0\overset{\circ}{.}7\ \mathrm{yr}^{-1}$ estimated by Ozernoy et al. (2000), where the model planet semimajor axis is ~60 AU rather than ~40 AU. Our model planet is located to the north of the star, rather than to the west of the star. Our model planet mass is similar to theirs but at a moderate eccentricity. Our model dust concentrations are a result of segregation in the phase of a resonant angle rather than caused by a large libration amplitude. Furthermore, because of the eccentricity of the planet, our model predicts that the morphology of the dusty ring will vary as well as revolve as the planet orbits about the star.

The initial conditions of our simulations cause many of the particles to be trapped in the resonances and at fairly low eccentricity. It is possible that low-eccentricity planetesimals exist in the system and that they are the source of the dust

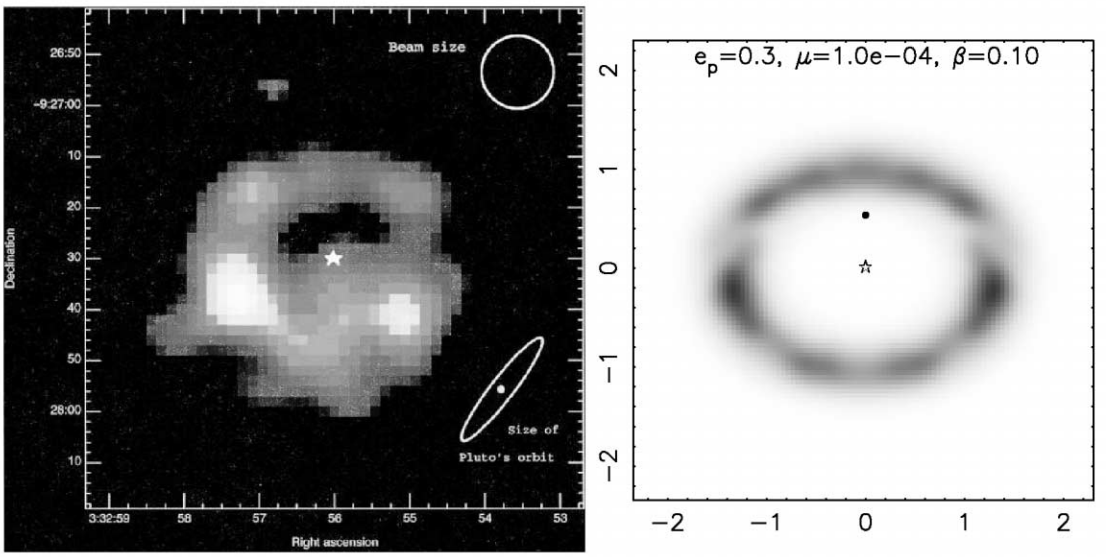

FIG. 2.—*Right*: Simulated intensity distribution based on the simulation shown in Fig. 1*a* for a 0.3 eccentricity planet at periastron of a planet to stellar mass ratio of 10^{-4}. *Left*: For comparison, the 850 μm submillimeter emission map of the ϵ Eri system (this is Fig. 1 of Greaves et al. 1998). The location of the star is denoted in both panels as a star symbol. For the simulated intensity distribution, we have chosen a disk inclination of 40°, where 0° is face-on. The dust distribution has been weighted by r^{-2} to simulate the intensity field from the star and then smoothed to the approximate resolution of the submillimeter images. We estimate that the planet is currently located to the north of the star (*right panel*; *filled circle*) at a declination of about −9°27′20″ (epoch 1998, as from Fig. 1 of Greaves et al. 1998). Axes for the simulation are given in units of the semimajor axis of the planet. [*See the electronic edition of the Journal for a color version of this figure*.]

particles that we see. Alternatively, the planetesimals in the system are farther out and the dust particles become trapped in the resonances as they spiral in toward the planet. Further simulations would be required to differentiate between these possibilities. In either case, resonant capture into these resonances is less likely and less prolonged when the planet mass or eccentricity is high. If the planet mass is too low, then it cannot be responsible for clearing a gap or central region in the dust distribution. Additional and more massive planets would be required to do this.

It is possible that high-eccentricity planets are common in the outskirts of extrasolar systems. If so, then the resulting dust distributions would not only revolve (Ozernoy et al. 2000) but would also be dependent on the orbital phase of the planets. This is an exciting prospect because there would be variations in the dust morphology on observable timescales.

This work would not have been carried out without helpful discussions with Joel Green and Dan Watson. This project was supported in part by NSF award PHY-9987413 for the REU program at the University of Rochester.

REFERENCES

Aumann, H. H., et al. 1984, ApJ, 278, L23
Burns, J. A., Lamy, O. L., & Soter, S. 1979, Icarus, 40, 1
Dermott, S. F., Jayaraman, S., Xu, Y. L., Gustafson, B. A. S., & Liou, J. C. 1994, Nature, 369, 719
Greaves, J. S., et al. 1998, ApJ, 506, L133
Holland, W. S., et al. 1998, Nature, 392, 788
Jayawardhana, R., Fisher, S., Hartmann, L., Telesco, C., Pina, R., & Fazio, G. 1998, ApJ, 503, L79
Koerner, D. W., Ressler, M. E., Werner, M. W., & Backman, D. E. 1998, ApJ, 503, L83
Liou, J.-C., & Zook, H. A. 1999, AJ, 118, 580
Moro-Martin, A., & Malhotra, R. 2002, AJ, in press (astro-ph/0207350)
Ozernoy, L. M., Gorkavyi, N. N., Mather, J. C., & Taidakova, T. A. 2000, ApJ, 537, L147
Saar, S. H., & Osten, R. A. 1997, MNRAS, 284, 803
Schneider, G., et al. 1999, ApJ, 513, L127
Soderblom, D., & Dappen, W. 1989, ApJ, 342, 945
Song, I., Caillault, J.-P., Barrado y Navascués, D., Stauffer, J. R., & Randich, S. 2000, ApJ, 533, L41
Wilner, D. J., Holman, M. J., Kuchner, M. J., & Ho, P. T. P. 2002, ApJ, 569, L115